5th International Conference on Silicon Photovoltaics, SiliconPV 2015

Reduction of thermomechanical stress using electrically conductive adhesives

Torsten Geipel[a],*, Li Carlos Rendler[a], Manuel Stompe[b], Ulrich Eitner[a], Lutz Rissing[b]

[a] *Fraunhofer Institute for Solar Energy Systems, ISE, Heidenhofstrasse 2, 79110 Freiburg, Germany*
[b] *Institute of Microproduction Technology, Leibniz University Hannover, An der Universitaet 2, 30823 Garbsen, Germany*

Abstract

We compare the thermomechanical stresses in solar cell interconnections based on electrically conductive adhesives (ECA) with soldered joints by using bending experiments and finite element analysis (FEA). Additionally, the influence of an increasing number of busbars is studied. The FEA is validated by measuring the bending of cell strips after cooling down from a single-sided interconnection process. The material parameters are determined by tensile tests, microscopy and nanoindentation. The comparison of ECA and soldering shows that an elastomer with a Young's modulus of below 0.5 GPa is capable of reducing the thermomechanical stress effectively resulting in, approximately, a mean tensile stress in the ECA of 5 MPa, 110 MPa in the ribbon, and a maximum compressive stress in the silicon of 75 MPa. Increasing the number of busbars from three to five leads to a reduction in compressive stresses in the silicon and a slight increase of the peak tensile stress in the busbars.

Keywords: Photovoltaic Module; Interconnection; Electrically Conductive Adhesives; Thermomechanical Stress; Finite Element Model

1. Introduction

New high-efficiency cell concepts such as heterojunction solar cells reach efficiencies well above 24% [1]. These concepts require a low temperature interconnection process to manufacture modules due to the temperature sensitivity of the involved cell layers. Lead-based solders, as the present standard interconnection technology, need

* Corresponding author. Tel.: +49-761-4588-5023; fax:+49-761-4588-9193
 E-mail address: torsten.geipel@ise.fraunhofer.de

to be processed at temperatures above 200 °C which is not suited for the interconnection for temperature sensitive high-efficiency solar cells. Instead, glueing with conductive films [2] and conductive adhesives in form of pastes [3] have proven to be alternative solutions thanks to their low processing temperatures of below 180 °C. ECAs have become the key interconnection technology for the fabrication of metal-wrap-through solar modules [4]. Still, using ECAs as a replacement for soldering is mainly confined due to the higher material costs and lacking long-term experience

The interconnection process induces thermomechanical stress on the interconnection and the solar cell. This is due to the different contraction of the metal components of the interconnection as compared to the silicon wafer caused by the differences in coefficients of thermal expansion (see Table 1). As a result of their lower processing temperatures, using ECA can reduce the thermomechanical stress after the interconnection process [5].

Until present, the simulation work on crystalline silicon H-pattern solar cells focused on soldered interconnections with a successive refinement of model parameters and complexity [6–9]. The interest in thermomechanical stress analysis of ECA was driven by the development of long-term stable backcontact modules [10–13]. Due to the availability of a large variety of ECAs with widely differing material properties it is important to question which material properties are important in order to reduce the thermomechanical stress effectively.

There is a trend to increase the number of interconnections per cell in order to reduce the series resistance [14]. However, it has not been investigated so far which changes in thermomechanical stress will arise due to the introduction of more than three busbars.

Thus, it is our goal to understand the effects of the mechanical properties of ECAs for the reduction of thermomechanical stress on the solar cell interconnection and compare the effects with standard leaded soldering. Additionally, we want to understand the thermomechanical stress for an increasing number of busbars. Therefore, we want to establish and validate a finite element model with appropriate material parameters for the interconnection with different interconnection technologies.

Nomenclature

CTE	Coefficient of thermal expansion
E	Young's modulus
E_x	Young's modulus (with x the respective layer)
E_t	Tangent modulus in plastic region
σ	Stress from tensile stress-strain curves
σ_{ys}	Yield strength
σ_I	1st principal stress
σ_{II}	3rd principal stress
σ_x	Normal stress in x-direction
σ_y	Normal stress in y-direction
v	Displacement in y-direction
z	Depth
ε	Strain from tensile stress-strain curves
t_x	Layer thickness (with x the respective layer)

---

2. Approach

The approach for the investigation is to create a finite element model (FEM) of single-sidely interconnected cell strips and calculate the cell bending for the case of two different adhesives: a thermoset adhesive (Young's modulus $E \approx 5$ GPa) and an elastomer adhesive ($E \approx 9$ MPa) and two different processing temperatures (130 °C and 160 °C) as well as interconnection by leaded solder with a solidification temperature of 179 °C. The dimensions of the components are obtained using optical microscopy and scanning electron microscopy. The mechanical parameters of

bulk adhesive samples and copper ribbons are gathered using tensile tests. Nanoindentation [15] is applied to mechanically characterize the metallization pastes of the solar cells. The model parameters are validated by comparing the calculated bending with the bending of experimentally manufactured cell strips. After validation, models of three to five busbar solar cells with front and rear interconnection are designed and used to study the thermomechanical stress of ECAs in comparison to soldered interconnections.

3. Materials and methods

3.1. Preparation of cell strips and measurement of the cell bending

The cell strips for measuring the cell bending and validation of the FEM are prepared from mono-crystalline solar cells merely having busbars at the front side. The solar cells are laser-cut into pieces of 45 mm × 20 mm. The cell strips are interconnected using different interconnection methods and temperatures with three to four pieces per group:

- thermosetting ECA cured at 160 °C
- thermosetting ECA cured at 130 °C
- elastomeric ECA cured at 160 °C
- elastomeric ECA cured at 130 °C
- solder reference with solidification temperature of 179 °C

The measurement of the cell bending is done with a chromatic confocal sensor. The measurement is done three days after preparing the samples such that some stress has already been relaxed due to the viscoelastic material behaviour.

3.2. Tensile tests

Tensile tests are performed to obtain the mechanical parameters of the adhesives. Bulk pieces of ECA are prepared on a heating plate using a flexible PTFE sheet as a substrate and polyimide tape to create moulds on the substrate in which the ECA is squeezed into. After curing at 150 °C for 30 min the larger bulk pieces of ECA are cut and sanded into stripes of approximately 4.0 mm × 40 mm × 0.35 mm which are used for the tensile tests. Eight to ten stripes are tested for each ECA.

The ribbon specimen for the tensile tests are cut from the spool in a length of 160 mm and are not stretched. The ribbons are $Sn_{62}Pb_{36}Ag_2$-coated and have dimensions of 1.5 mm × 0.2 mm.

The tensile tests are done on a Zwick/Roell tensile testing machine equipped with a video extensiometer for contactless strain determination avoiding the influence of the machine stiffness. The clamping length of the ECA is 15 mm. It is 100 mm for the ribbons. The initial measurement length is approximately 10 mm for ECA and 20 mm for the ribbon. The cross head has a constant speed of 1 mm/min in the case of ECA and 1.5 mm/min in the case of the copper ribbon in the range of the Young's modulus determination.

Representative stress-strain curves of the thermosetting ECA and the elastomeric ECA are presented in Fig. 1a. Fig. 1b shows a detail of the stress-strain curve of the elastomeric ECA. Both types of ECA show significantly different mechanical behavior. Whereas the thermoset dominantly shows a linear elastic behavior with comparably high failure stress (30 – 50 MPa) but low failure strain (0.3 % – 1 %), the elastomer has a linear elastic region up to a yield point ($\sigma_{ys} \sim 1.4$ MPa) and continues straining at almost constant stress level until failure at a comparably high failure strain (60 % – 100 %).

a)

b)
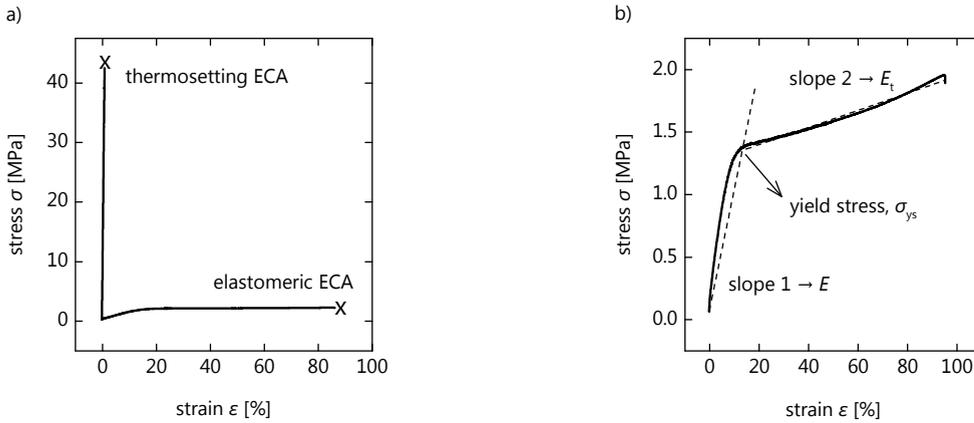
Fig. 1. Stress-strain curves of a) the thermoset and the elastomer, and b) shows a detail of the stress-strain curve of the elastomer with illustrations of the determination of the elastic-plastic mechanical parameters.

3.3. Nanoindentation

The mechanical properties of the silver and aluminium paste is determined by nanoindentation [15]. The measurement tip is a Berkovich diamond (three-faced pyramid) with a radius of 80 nm. The indendation depth is 100 to 150 nm. The force is applied within 5 s and the dwell time is 3 s to mitigate dynamic effects. The measured indentation force for the paste is 100 – 200 µN and for the silicon at 1500 µN. Nanoindentation measurements are performed on a total of four different cell types to gain insight into the variation among different cells. Fig. 2 shows the results of the measurements. Cell type 2 is the cell type used for the bending experiments presented in this paper. The varying parameters among different cell types is explained by the different pastes used on the cells. The scatter within one group is assumed to be caused by local differences in the mechanical properties of the pastes due to their nonuniform and porous nature.
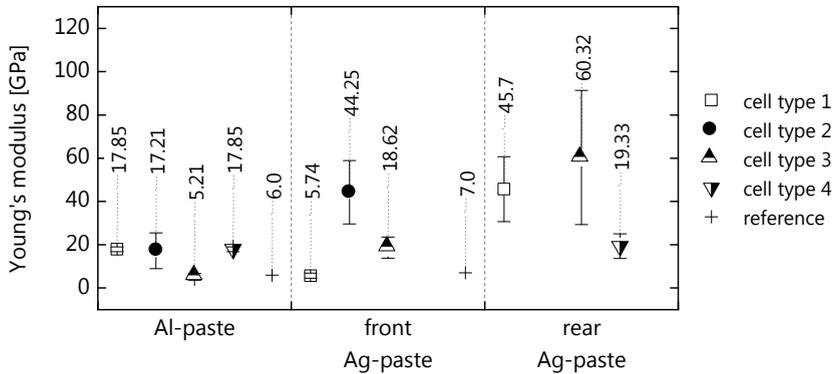
Fig. 2. Young's modulus of the metallization pastes as determined by nanoindentation. The reference values are taken from [8]. Error bars represent standard deviations of four to five consecutive measurements.

3.4. Optical microscopy and scanning electron microscopy

The thickness of the silicon, metallization and adhesive layers is determined by cross sectioning a sample cell strip and analyzing with optical microscopy and scanning electron microscopy.

3.5. Finite element model

The FEM of the three to five busbar solar cell is desinged via reducing the complete geometry to a symmetry element in form of a quarter cell as shown in Fig. 3a. The symmetry element has a fixed boundary condition in one corner and a roller boundary condition at the lower ribbon surfaces at the rear side. An overview of the three different geometries for the increasing number of busbars can be seen in Fig. 3b and a detailed view of the meshing is shown in Fig. 3c. The meshing degree for the simulation is chosen as a compromise between accuracy and reasonable calculation speed resulting in between 200,000 to 400,000 volume elements. This compromise leads to an underestimation of stress singularities but does not impede the capability of the model to compare the different interconnection technologies with each other.

The stress-free state is chosen to be the solidification temperature of each interconnection technology, which is 179 °C for soldering and 160 °C for the glues. The stressed state is defined at room temperature, 22 °C. A stationary calculation is done without time-dependent effects such as creep. Minor geometrical simplifications to the actual cell design are made to improve meshing and convergence such as omitting the upper solder layer and setting the rear busbar thickness to the thickness of the sintered aluminium layer. An overview of the material input parameters to the FEM as determined with the techniques explained above or taken from literature is given in Table 1.
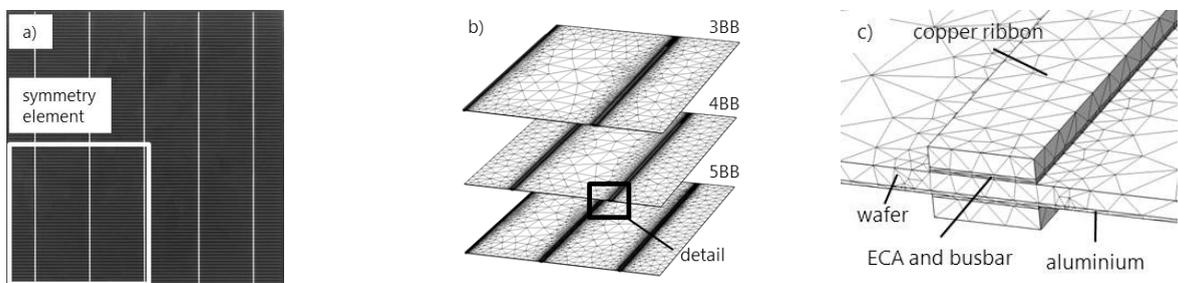
Fig. 3. a) Illustration of the chosen symmetry element for the calculation. b) Overview of the FEM for the consecutive busbars, and c) detailed view on the layer structure and the mesh.

4. Results and discussion

4.1. Model validation

Fig. 4a shows the setup for the bending measurement with the chromatic confocal sensor. The results of the measured bending of the cell strips are presented together with the calculated bending in Fig. 4b. It can be seen that the simulation is in good agreement with the experiment, so we conclude that the material parameters are suitable to describe the solar cell interconnection and to compare different interconnection technologies with each other. The uncertainty of the simulation (error bars in Fig. 4b) is caused by the uncertainties of the input parameters as given in Table 1. Using the propagation of uncertainty it is shown that the uncertainty of the Young's modulus of the aluminium paste has the main influence on the variation of the calculated cell bending. The model seems to slightly overestimate the cell bending due to the missing creep effects in the solder and adhesive layer.

Table 1. Overview of the material parameters used in the FEM simulation.

	Constitutive model	Young's modulus E [GPa]	Yield Strength σ_{ys} [MPa]	Tangent modulus E_t [GPa]	Poisson ratio	Density [kg/m³]	CTE [ppm/K]
thermoset	linear elastic	5.2 ± 0.5	n.a.	n.a.	0.38 [16]	3000 [datasheet]	40 [datasheet]
elastomer	bi-linear plastic	$8.5\times10^{-3} \pm 0.3\times10^{-3}$	1.4 ± 0.1	$2\times10^{-4} \pm 3\times10^{-5}$	0.49 [estimate]	2400 [estimate]	370 [datasheet]
solder	bi-linear plastic	32.0 [17]	48.0 [17]	2.4 [18]	0.4 [19]	8600 [19]	25.2 [17]
ribbon	bi-linear plastic	81.2 ± 3.8	100.7 ± 0.3	1.7 ± 0.1	0.34 [19]	8930 [19]	16.4 [19]
silver busbar	linear elastic	44.3 ± 14.7	n.a.	n.a.	0.3[20]	8580 [21]	10.4 [22]
wafer	orthotropic	reference [23]				2329 [19]	2.49 [19]
aluminium paste	linear elastic	17.3 ± 8.3	n.a.	n.a.	0.3 [20]	2700 [estimated]	15.9 [22]
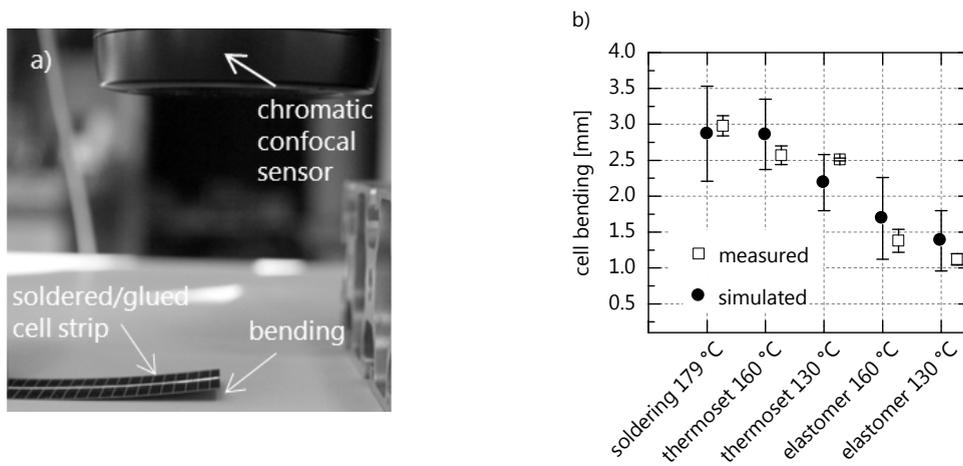
Fig. 4. a) Measurement setup for the experimental determination of the cell bending. b) Comparison between measured and simulated bending for different interconnection methods and temperatures. The errors bars at the experimental data represent standard errors of the mean. The error bars at the simulated values denote uncertainties of the simulation caused by uncertainties in the input parameters as given in Table 1.

4.2. Calculation of stresses from the interconnection process

In Fig. 5 cross sections of the modeled interconnection are presented. Fig. 5a) shows the normal stress in y-direction. Positive values, which indicate tensile stresses, are presented in dark gray. We find the copper ribbon, the solder/ECA-layer and the busbar components to be afflicted with tensile stress. On the contrary, Fig. 5b shows the normal stress in x-direction for the same cross section. Here, the dark gray areas indicate negative stress values in the region of the silicon underneath the busbar signifying compressive stress. Moreover, tensile stress exists at the edges of the busbar-solder/ECA-interface and at the edges of the busbar-silicon interface.

a)

b)

Fig. 5. a) Cross section of the interconnection with the normal stress in y-direction highlighted. b) The same cross section with the normal stress in x-direction.

a)

b)
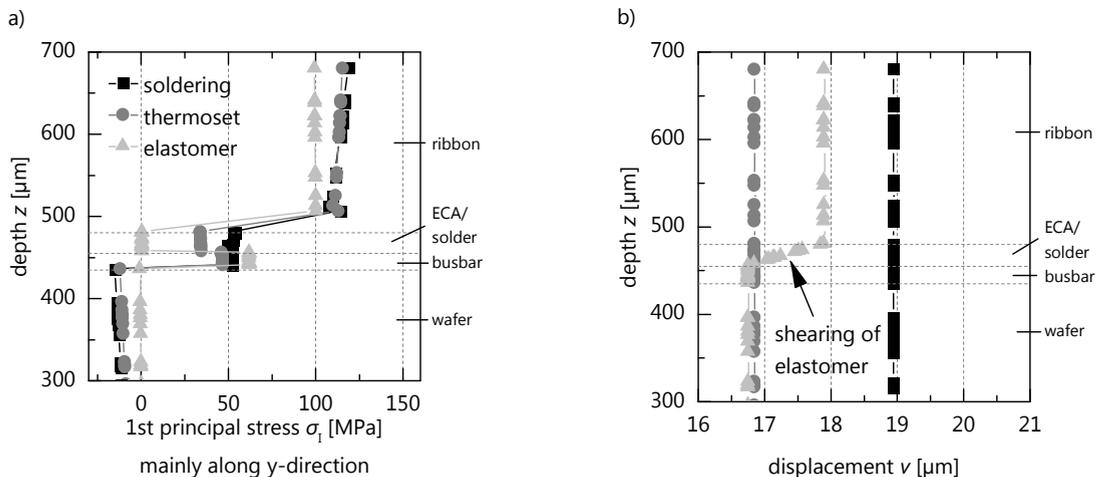
Fig. 6a) 1st principal stress along the depth of the interconnection (only sunny side shown). The elastomer leads to a reduction in the stress in the ribbon and wafer. The thermoset leads to similar stress as soldering. b) Displacement in y-direction. The stress in the interconnection is relaxed in the elastomer via a shear displacement.

To understand the stress distribution with different interconnection methods, σ_I along the depth z of the interconnection is shown in Fig. 6a. By using a thermosetting adhesive cured at 160 °C instead of soldering the thermomechanical stress in the intermediate layer is reduced from 50 to 40 MPa. If an elastomeric adhesive is used, the stress in the ECA-layer can be lowered to approximately 1 MPa.

The stress in the ribbon is almost identical in the case of the thermosetting ECA compared to soldering and is reduced from 120 MPa to 100 MPa if an elastomer is applied instead. The large stress reduction in the elastomer is due to a shear displacement in the ECA, which absorbs the stress caused by the CTE-mismatch between copper and silicon (see Fig. 6b).

Fig. 7a to d show histograms of the stress distribution in the interconnection components for the ECAs and soldering as reference. The case of a three busbar interconnection is considered. Fig. 7a to d indicate that using the thermoset can only slightly reduce the stress peaks. The elastomer efficiently narrows and lowers the stresses in all components. In the silicon the compressive stress is lowered from −200 MPa to −50 MPa if the elastomer is used. In the copper ribbon the tensile stress is narrowed and reduced from 120 MPa to 100 MPa.

The remaining high stresses if using a thermoset are also noticable via the high amount of bending after interconnection. Due to the fact that the thermoset can be cured at lower temperatures than 160 °C, it may still be

useful to reduce the thermomechanical stress. However, in all cases, where very low thermomechanical stress is required it is advisable to use an elastomer that allows the absorption of thermomechanical stress.

It is commonly known that relaxation of thermomechanical stress takes place in the hours and days after the interconnection process. Therefore, it is assumed that stress peak values are 30 – 50 % lower if time-dependent effects are included into the model [8].
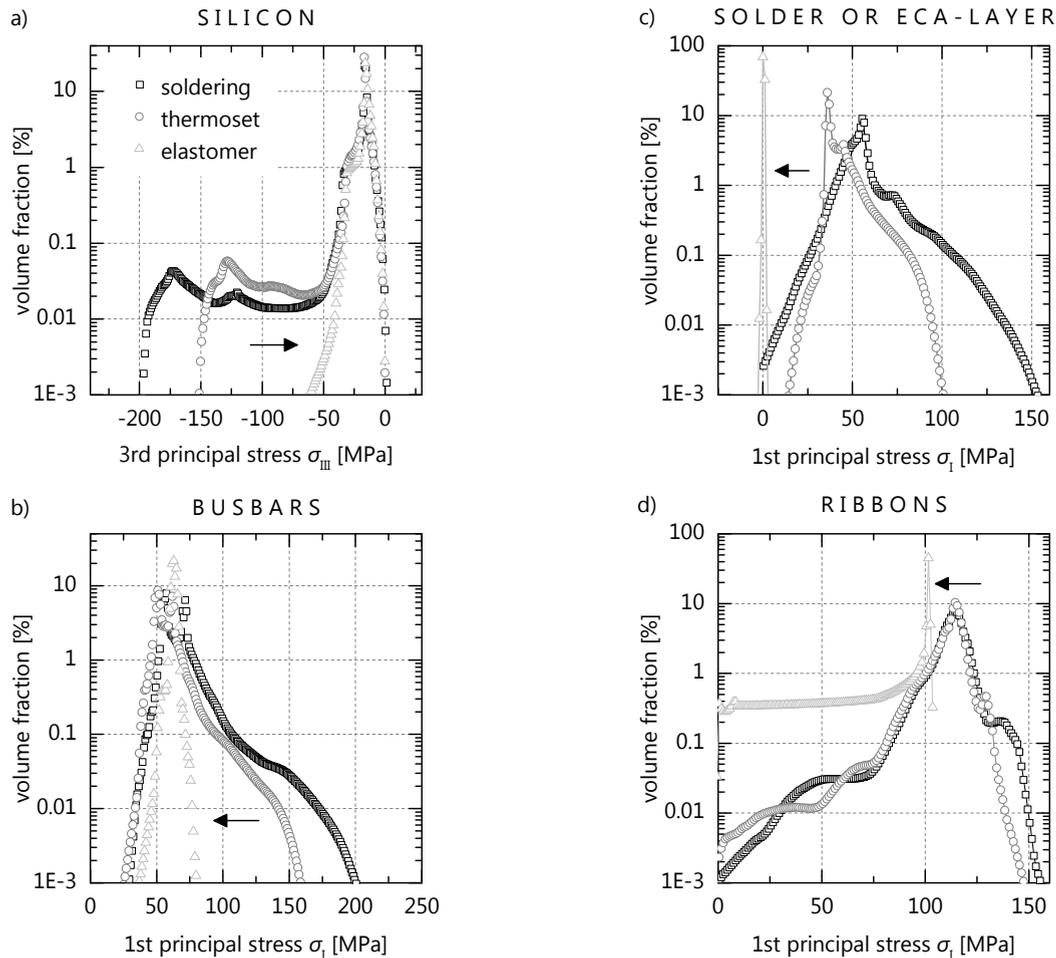
Fig. 7. a-d) Stress distributions in the interconnection components for varying interconnection technologies. The arrows indicate the stress reduction by the elastomeric adhesive.

It is now the aim to find a threshold value for the Young's modulus of the ECA which supports the reduction of the stress in the interconnection components. A parameter variation of the Young's modulus of the thermoset ECA is performed (without plasticity) and the resulting stress distributions in the components are analyzed.

In Fig. 8a to c it can be observed, that the reduction of the Young's modulus of the ECA leads to a merging and narrowing of the distributions into approximately a single distribution. When using $E \approx 0.5$ GPa, the compressive stress in the silicon can be reduced to a minimum of −75 MPa, in the ribbon to a maximum of 110 MPa and in the ECA to 5 MPa. For $E < 0.5$ GPa the changes in the stresses are not considered to be significant. Please note, that this result is constraint to this specific cell and material setup.

a)   SILICON

b)   ECA

c)   RIBBON
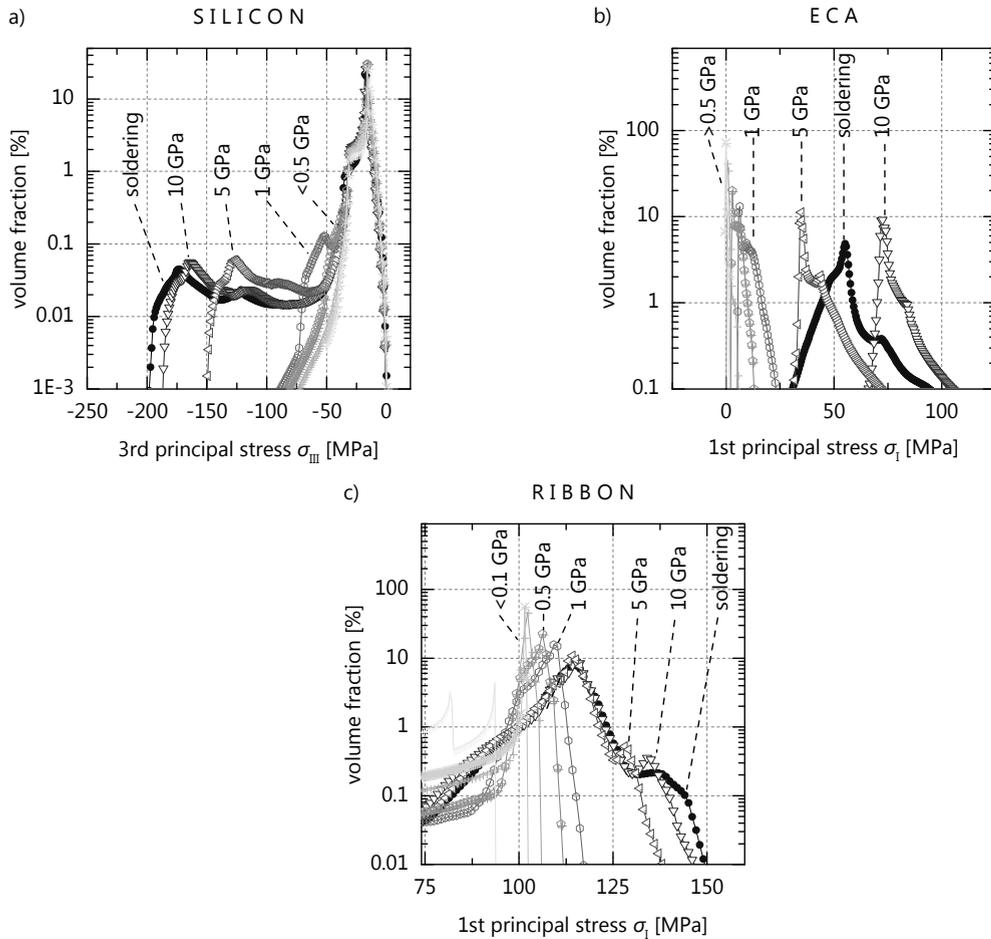
Fig. 8a-c) Stress distributions in the interconnection components for a varying Young's modulus of the ECA. The stress distributions merge with decreasing Young's modulus. The stress is significantly reduced if the Young's modulus of the ECA is below 0.5 GPa.

The thermomechanical stress within soldered interconnections is investigated for an increasing number of busbars. The results of the study is that few changes occur in σ_{III} in the silicon and σ_I in the busbars. σ_{III} is slightly higher (meaning less compressive stress) with an increasing number of busbars. The minium value in the case of three busbar is approximately −200 MPa, and −160 MPa in the case of five busbars. The σ_I in the busbars increases with increasing number of busbars. Peak σ_I can reach up to 225 MPa in the case of 5BB and is limited to 200 MPa in the case of three and four busbars. The different σ_{III} in the silicon is considered uncritical whereas the increasing σ_I in the busbars may have an influence on the probability of crack initiation in the interconnection.

5. Conclusion

A finite element model for the interconnection of crystalline silicon H-pattern solar cells is established to study to the thermomechanical stress of glueing in comparison to soldering, and to investigate the effects of an increasing number of busbars. The model is validated by comparing measured and simulated bending of cell strips.

It is found that the compressive stresses in the silicon and tensile stresses in the busbar, solder or ECA and ribbon are prevailing after the interconnection process due to different contraction of materials caused by the CTE-mismatch between copper and silicon. The elastomeric ECA can reduce stress peaks due to its ability to deform plastically and therefore absorb the stresses, whereas the thermosetting ECA still leads to major stress peaks comparable to soldering. A parameter variation shows that an elastomeric ECA with a Young's modulus of < 0.5 GPa is able to diminish the stress efficiently. It is found that an increasing number of busbars leads to a slight reduction of compressive stresses in the silicon and increase in tensile stress in the busbars.

References

[1] Taguchi M, Yano A, Tohoda S, Matsuyama K, Nakamura Y, Nishiwaki T, Fujita K, and Maruyama E. 24.7% Record Efficiency HIT Solar Cell on Thin Silicon Wafer. IEEE J. Photovoltaics 2014; 4: 96–99

[2] Choi J, Kim S, Lee J, Park H, Lee W, and Cho E. Advanced module fabrication of silicon heterojunction solar cells using anisotropic conductive film method. 26th EUPVSEC. 2011, pp. 3302–3304.

[3] Späth M, Veldman D, Dekker NJ, Bennett IJ, Eerenstein W, Jong PC de, Ribeyron PJ, Harrison S, and Munoz D. Hetero-junction module technology. 26th EUPVSEC. 2011, pp. 3121–3124.

[4] Lamers M, Tjengdrawira C, Koppes M, Bennett I, Bende EE, Visser TP, Kossen E, Brockholz B, Mewe AA, and Romijn IG. 17.9% Metal-wrap-through mc-Si cells resulting in module efficiency of 17.0%. Prog. Photovolt: Res. Appl. 2012; 20: 62–73

[5] Bennett IJ, de Jong, P. C, Kloos MJ, Stam CN, Henckens A, Schuermans J, Gomez RJ, Sánchez-Friera P, Lalaguna B, and Schmidt H. Low-stress interconnection of solar cells. 22nd EUPVSEC. 2007, pp. 2674–2678.

[6] Wiese S, Meier R, Krämer F, and Bagdahn J. Constitutive behaviour of copper ribbons used in solar cell assembly processes. 10th EuroSimE. 2009, pp. 1–8.

[7] Wiese S, Krämer F, Meier R, and Schindler S. Mechanical problems of manufacturing processes for photovoltaic modules. 18th EMPC. 2011, pp. 1–6.

[8] Krämer F, Seib J, Peter E, and Wiese S. Mechanical stress analysis in photovoltaic cells during the string-ribbon interconnection process. 15th EuroSimE. 2014, pp. 1–7.

[9] Dietrich S, Pander M, Sander M, and Ebert M. Mechanical investigations on metallization layouts of solar cells with respect to module reliability. Energy Procedia 2013; 38: 488–497

[10] Eikelboom, D. W. K, Bultman JH, Schonecker A, Meuwissen, M. H. H, van den Nieuwenhof, M. A. J. C, and Meier DL. Conductive adhesives for low-stress interconnection of thin back-contact solar cells. 29th IEEE PVSC. 2002, pp. 403–406.

[11] Meuwissen M, van den Nieuwenhof, M, Steijvers H, Bots T, Broek K, and Kloos, M. J. H. Simulation Assisted Design of a PV Module Incorporating Electrically Conductive Adhesive Interconnects. 21st EUPVSEC. 2006, pp. 2485–2490.

[12] Meuwissen M, van den Nieuwenhof, M, Steijvers H, van der Waal, A, and Bots T. Validation of constitutive models for electrically conductive adhesives. EuroSimE. 2007, pp. 1–8.

[13] Pander M, Schulze S, and Ebert M. Mechanical modeling of electrically conductive adhesives for photovoltaic applications. 29th EUPVSEC. 2014, pp. 3399–3405.

[14] Chunduri. The buzz on busbars. Photon International 2013; September: 84–105

[15] Stompe M, Cvetković S, Pape F, and Rissing L. Mechanical characterization of machining results for sintered silicon-carbide (SSiC). 11th euspen International Conference. 2011, pp. 357–360.

[16] Kahraman R, Sunar M, and Yilbas B. Influence of adhesive thickness and filler content on the mechanical performance of aluminum single-lap joints bonded with aluminum powder filled epoxy adhesive. J. Mater. Process. Technol. 2008; 205: 183–189

[17] Wiese S, Krämer F, Peter E, and Seib J. Mechanical problems of novel back contact solar modules. 13th EuroSimE. 2012, pp. 1–6.

[18] Jendrny J, Müller WH, and Albrecht H. Strength and lifetime analysis of SMT solder joints: An exemplary study of the MiniMELF component. Surface Mount International 1997. 1997, pp. 626–636.

[19] MatWeb: Material Property Data. 2014. Available: www.matweb.com.

[20] Popovich V, "Microstructure and mechanical aspects of multicrystalline silicon solar cells" . Dissertation. Delft University of Technology. 2013.

[21] Bai G, "Low-temperature sintering of nanoscale silver paste for semiconductor device interconnection" . Dissertation. Virginia Polytechnic Institute and State University. 2005.

[22] Kohn C, Faber T, Kübler R, Beinert J, Kleer G, Clement F, Erath D, Reis I, Martin F, and Müller A. Analyses of warpage effects induced by passivation and electrode coatings in silicon solar cells. 22nd EUPVSEC. 2007, pp. 1270–1273.

[23] Hopcroft MA, Nix WD, and Kenny TW. What is the Young's Modulus of Silicon? J. Microelectromech. Syst. 2000; 19: 229–238